European Journal of Pharmaceutics and Biopharmaceutics 129 (2018) 111–121

Contents lists available at ScienceDirect

European Journal of Pharmaceutics and Biopharmaceutics

journal homepage: www.elsevier.com/locate/ejpb

Research paper

Development of PLGA nanoparticle loaded dissolving microneedles and comparison with hollow microneedles in intradermal vaccine delivery

Juha Mönkäre[a], Maria Pontier[a], Eveline E.M. van Kampen[a], Guangsheng Du[a], Mara Leone[a], Stefan Romeijn[a], M. Reza Nejadnik[a], Conor O'Mahony[b], Bram Slütter[a], Wim Jiskoot[a], Joke A. Bouwstra[a,*]

[a] Division of BioTherapeutics, Leiden Academic Centre for Drug Research (LACDR), Leiden University, P.O. Box 2300, Einsteinweg 55, 2333 CC Leiden, The Netherlands
[b] Tyndall National Institute, Lee Maltings Complex, University College Cork, Dyke Parade, T12R5CP Cork, Ireland

ARTICLE INFO

Keywords:
Dissolving microneedles
Skin immunisation
Vaccine delivery
Particulate vaccines
PLGA nanoparticles

ABSTRACT

Skin is an attractive but also very challenging immunisation site for particulate subunit vaccines. The aim of this study was to develop hyaluronan (HA)-based dissolving microneedles (MNs) loaded with PLGA nanoparticles (NPs) co-encapsulating ovalbumin (OVA) and poly(I:C) for intradermal immunisation. The NP:HA ratio used for the preparation of dissolving MNs appeared to be critical for the quality of MNs and their dissolution in *ex vivo* human skin. Asymmetrical flow field-flow fractionation and dynamic light scattering were used to analyse the NPs released from the MNs *in vitro*. Successful release of the NPs depended on the drying conditions during MN preparation. The delivered antigen dose from dissolving MNs in mice was determined to be 1 μg OVA, in NPs or as free antigen, by using near-infrared fluorescence imaging. Finally, the immunogenicity of the NPs after administration of dissolving MNs (NP:HA weight ratio 1:4) was compared with that of hollow MN-delivered NPs in mice. Immunization with free antigen in dissolving MNs resulted in equally strong immune responses compared to delivery by hollow MNs. However, humoral and cellular immune responses evoked by NP-loaded dissolving MNs were inferior to those elicited by NPs delivered through a hollow MN. In conclusion, we identified several critical formulation parameters for the further development of NP-loaded dissolving MNs.

1. Introduction

Skin is an attractive site for vaccination because of its rich network of immune cells and its accessibility [1]. However, the top layer of the skin, the stratum corneum, effectively prevents the penetration of vaccines into the skin. Conventional needles can be used for intradermal immunizations but this method is painful and technically challenging. Therefore, vaccination via the skin requires the development of a device that enables pain-free administration of vaccines into the epidermis and dermis, which both harbour a dense network of immune cells (e.g. Langerhans cells and dermal dendritic cells) [2]. Among several developed devices for intradermal vaccine administration, microneedles (MN) are currently one of the most promising technologies. They are needle-like structures with micron-scale lengths (< 1000 μm) typically assembled as arrays with the ability to pierce into the skin in a minimally invasive and pain-free manner [3,4].

In modern vaccine programmes, subunit antigens (e.g., proteins) are preferred since they can offer safer and better controlled alternatives to whole vaccines [5,6]. However, frequently the immunogenicity of plain subunit antigens is limited. Therefore, subunit vaccines typically contain adjuvants, such as an optimally designed delivery system and an immune modulator. Several types of nanocarriers have been examined for vaccine delivery and of those polymeric nanoparticles (NP) and liposomes are most commonly used [7–9]. Particle-based vaccines can improve the immune responses against the antigen due to their resemblance to pathogens, prolonged release of antigen and possibility to tailor particle properties depending on the required type of immune response [5,8,10]. In addition, particulate formulations allow the co-delivery of antigen and adjuvant and enhanced uptake in DCs, which can further enhance the immunogenicity of the antigen against infectious diseases [11–13] or cancer [14–16]. However, the skin is still rarely used as non-invasive administration route for particulate vaccines. The major challenges are reproducible delivery of a sufficient dose of particulate vaccines into the skin and simultaneous the minimization of the fabrication wastage of the vaccine.

Arrays of dissolving [17,18] and coated MNs [19] are dry-state MN technologies that have been used to deliver NP vaccines into the skin. In dissolving MNs, nanoparticles are localized in the MN matrix, and after

* Corresponding author.
E-mail address: bouwstra@lacdr.leidenuniv.nl (J.A. Bouwstra).

https://doi.org/10.1016/j.ejpb.2018.05.031
Received 14 March 2018; Received in revised form 18 May 2018; Accepted 23 May 2018
Available online 24 May 2018

the MN array is inserted into the skin, the MNs dissolve, thereby releasing the NPs. Beside dry-state MNs, single hollow MN can be used to inject NP suspensions into the skin without time-consuming development of dissolving or coated MN formulations. Therefore, it is an ideal tool to compare vaccine formulations for intradermal delivery [20].

The advantages of dissolving MNs are that the use of dry vaccine formulations can potentially increase the stability and eliminate the need for a cold chain, in contrast to hollow MNs which require a liquid formulation [21,22]. In addition, dissolving MNs are prepared from safe and biodegradable materials and do not create sharp waste in contrast to coated MNs [4]. Until now, a limited number of studies have been reported on NP-based intradermal vaccination using dissolving MNs [17,18]. Particularly, the formulation development of NP-loaded dissolving MNs has not been described in detail in the literature. Moreover, studies on the effect of the MN composition and the NP incorporation on the preparation and MN dissolution have not been reported yet. Finally, the quantification of the intradermally delivered antigen dose are only reported for coated MNs [23]. Challenging factors for developing dissolving MNs include the need for (1) reproducible MN penetration into the skin, (2) dissolution and subsequent release of NPs from the MNs into the skin, (3) delivery of a sufficient and reproducible antigen dose and (4) minimizing the loss of often expensive antigen and adjuvant.

The aim of this study was to develop NP-loaded dissolving MNs to evoke humoral and cellular immune responses after intradermal vaccination. Poly(lactic-co-glycolic) acid (PLGA) NPs co-encapsulating model antigen ovalbumin (OVA) and TLR3 ligand poly(I:C) as adjuvant were selected. Dissolving MNs were prepared from hyaluronan (HA) and contained PLGA NPs that were loaded exclusively into the MN tips. Next, the most suitable formulation composition (i.e., the weight ratio of HA and NPs) and preparation conditions for MN dissolution was evaluated by using *ex vivo* human skin. Using the optimized MN composition, we quantified the delivered dose in mice. Finally, dissolving and hollow MN-mediated intradermal immunization with PLGA NPs were compared for the ability to evoke humoral and cellular immune responses in mice.

2. Materials and methods

2.1. Materials

Hyaluronan (sodium hyaluronate, average M_w was 150 kDa) was purchased from Lifecore Biomedical (Chaska, MN, USA). Alexa Fluor 647® NHS ester (AF647) was purchased from Life Technologies (Eugene, OR, USA). IRDye® 800CW protein labelling kit was ordered from LI-COR Biosciences (Lincoln, NE, USA). Polydimethylsiloxane (PDMS, Sylgard 184) was obtained from Dow Corning (Midland, MI, USA). Solid silicon MN arrays were kindly provided by the Tyndall Institute (Cork, Ireland). PLGA (50/50, acid terminated, M_w 24–38 kDa), ovalbumin for *in vitro* and *ex vivo* studies, bovine serum albumin (BSA), fluoresceinamine (isomer I, FAM), polysorbate 80 (Tween 80) were purchased from Sigma-Aldrich (St. Louis, MO, USA). Ethyl acetate was obtained from Boom Chemicals (Meppel, The Netherlands). Polyvinyl alcohol 4–88 (PVA, 31 kDa) was ordered from Fluka (Steinheim, Germany). Dimethylsulfoxide (DMSO) was ordered from Biosolve BV (Valkenswaard, The Netherlands). Sodium dodecyl sulfate (SDS) from Merck Millipore (Hohenbrunn, Germany). Ovalbumin (Endofit, endotoxin-free), polyinosinic-polycytidylic acid (poly(I:C)) (low molecular weight) and rhodamine-labelled poly(I:C) were obtained from Invivogen (Toulouse, France). HRP-conjugated goat anti-mouse IgG1 and IgG2a were purchased from Southern Biotech (Birmingham, AL, USA). 3,3′,5,5′-tetra methyl benzidine (1-Step Ultra TMB) was ordered from ThermoScientific (Rockford, IL, USA). Fluorescently labeled antibodies specific for CD4, CD8, Thy1.2 and CD45.1 were ordered from eBioscience (San Diego, CA, USA). The Cytofix solution for T-cell analysis was purchased from BD Biosciences (San Jose, CA, USA). Cell culture medium consisted of Roswell Park Memorial Institute medium (RPMI) with 10% Fetal bovine serum (FBS), 1% L-glutamine and 1% Penicillin-streptamycin. FACS buffer was prepared by diluting 2% FBS in PBS.

2.2. PLGA nanoparticle preparation

The PLGA NPs were prepared by a double emulsion solvent evaporation method as described earlier [20]. To prepare the first water-in-oil (W/O) emulsion, either 75 µl OVA solution (20 mg/ml) for *in vitro* studies (OVA-NP) or 18.8 µl OVA (40 mg/ml), 75 µl poly(I:C) (46.7 mg/ml) and 10 µl rhodamine-labelled poly(I:C) (100 µg/ml) for immunisation studies (OVA-PIC-NP) were mixed with 1 ml of PLGA dissolved in ethyl acetate (25 mg/ml) by tip sonication (15 sec, 20 W, Branson sonifier 250, Danbury, CT, USA). For visualisation or quantification studies, 20% of OVA was replaced with OVA-AF647 or 100% of OVA was replaced with OVA-IR800, respectively. Next, 2 ml of 2% PVA 4–88 (31 kDa) solution was dispersed with the W/O emulsion by using tip sonication (15 sec, 20 W) to obtain a W/O/W double emulsion. Subsequently, this emulsion was dropwisely added to the 25 ml of 0.3% (w/v) PVA extraction medium (40 °C) under stirring. Next, the ethyl acetate was evaporated by using a rotavapor (Buchi rotavapor R210, Switzerland) for 3 h (40 °C, 150 mbar). Then the NPs were collected by centrifugation (AvantiTM J-20XP centrifuge, Beckman Coulter, Brea, CA) at 35,000*g* for 10 min and washed twice with water. Finally, PLGA NPs were dried in an ice condenser (Christ Alpha1-2, Osterode, UK) in freeze vacuum (−49 °C, 90 mbar) overnight and stored at −20 °C until use.

2.3. PLGA nanoparticle characterisation

Dynamic light scattering (DLS) (ZetaSizer Nanoseries ZS system, Malvern instruments, Worcestreshire, UK) equipped with a He-Ne laser (633 nm) was used to measure size and polydispersity index (PDI) of the NPs dispersed in pH 7.4 PBS (140 mM NaCl, 16 mM Na_2HPO_4, 2.9 mM KH_2PO_4, 5.5 mM KCl). The zeta potential was measured by laser Doppler electrophoresis (ZetaSizer Nanoseries ZS system) and samples were dispersed in HEPES buffer (5 mM, pH 7.4).

To determine OVA and poly(I:C) loading of the NPs, 1 mg dried nanoparticles were dispersed in 0.15 ml DMSO and incubated for 1 h at 37 °C. Next, 0.85 ml (determination of OVA) or 0.35 ml (determination of poly(I:C)) of 0.05 M NaOH with 0.5% (w/v) SDS was added to samples which were thereafter incubated for an additional 1 h at 37 °C. The calibration curves were prepared in mixtures of DMSO and NaOH/SDS. Micro BCA™ protein assay (Pierce Micro BCA™ protein Assay kit, ThermoFisher, Rockford, IL, USA) was used to measure the OVA concentration following the manufacturer's instructions and absorbance was determined with a Tecan infinite M1000 plate reader (Tecan Austria GmbH, Grödig, Austria). To analyse of poly(I:C) concentration, fluorescence of rhodamine-labelled poly(I:C) was measured by using the plate reader (λ_{ex} 545 nm/λ_{em} 576 nm).

The encapsulation efficiency (EE) and loading capacity (LC) of OVA and poly(I:C) in the nanoparticles were calculated as below:

$$\text{EE } \% = \frac{M_{loadedOVA/poly(I:C)}}{M_{totalOVA/poly(I:C)}} \times 100\% \quad (1)$$

$$\text{LC } \% = \frac{M_{loadedOVA/poly(I:C)}}{M_{NP+OVA+poly(I:C)}} \times 100\% \quad (2)$$

where $M_{loaded\ OVA/poly(I:C)}$ represents the mass of loaded OVA or poly(I:C), $M_{total\ OVA/poly(I:C)}$ is the total amount of OVA or poly(I:C) added to the formulations and $M_{NP+OVA+poly(I:C)}$ is the total weight of NPs, OVA and poly(I:C).

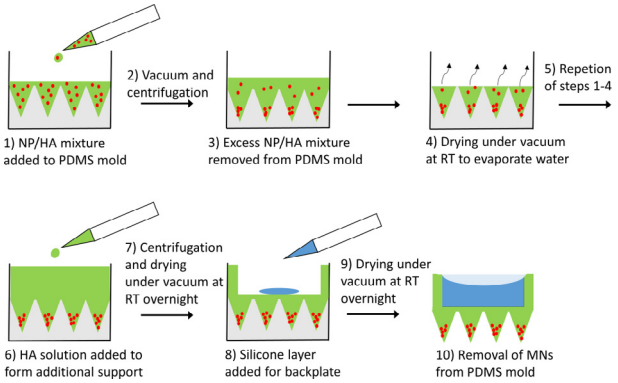

Fig. 1. Preparation scheme of NP-loaded dissolving MNs.

2.4. Dissolving microneedle preparation

The preparation scheme of the dissolving PLGA NP-loaded MNs is presented in Fig. 1. PDMS molds were prepared from silicon MN arrays (16 MN tips in 5.4 × 5.4 mm array, length 300 μm) as described earlier [24]. First, HA was dissolved overnight in 10 mM phosphate buffer (5.8 mM Na_2HPO_4, 4.2 mM NaH_2PO_4, pH 7.0). On the next day, NPs were suspended in buffer and HA solution and NP suspension were mixed so that the final concentrations of NPs and HA were 10 mg/ml and 10 mg/ml (NP:HA weight ratio 1:1), 5 and 20 mg/ml (NP:HA weight ratio 1:4) and 5 mg/ml and 50 mg/ml (NP:HA weight ratio 1:10), respectively. When MNs were visualized with fluorescence microscopy 1% of total HA was replaced with FAM-HA that was prepared as described earlier [24]. Next, 30 μl NP:HA mixture was pipetted into each array of the PDMS mold that was placed in the vacuum for 10 min to remove any entrapped air from the mixture (Fig. 1). To deposit the nanoparticles into the MN tips, the mold was placed into a centrifuge (Beckman Coulter Allegra X-12R Indianapolis, IN, USA) for 15 min at 3270*g*. After the centrifugation, the excess mixture (20–25 μl) was removed from the mold, and the remaining mixture was dried for 30 min in a vacuum desiccator at room temperature to evaporate the water. First four steps were repeated once by adding again NP:HA mixture (20 μl) into each array of PDMS, followed by centrifugation, removal of the excess mixture and drying. Subsequently, 60 μl of 50 mg/mL HA solution was added to form an additional HA layer, followed by centrifugation (30 min, 930*g*). Finally, the PDMS mold was dried overnight in a vacuum desiccator at room temperature. After the complete drying, a vaccine-free backplate was prepared for all MNs. A mixture of vinylpolysiloxane base and catalyst was prepared and it was added to each array to form the backplate [25]. MNs were stored at room temperature in a desiccator until use.

For *in vivo* studies, MNs containing only free OVA and poly(I:C) (free-OVA-PIC) were prepared, as follows: 60 μl solution containing HA (40 mg/ml), OVA (10 mg/ml) and poly(I:C) (10 mg/ml) was added to each array of the PDMS mold. This was placed in vacuum to remove any air and then centrifuged for 2 h at 3270*g*. After the centrifugation, another 60 μl of HA/OVA/poly(I:C) solution was added in arrays of the mold followed by the repetition of the centrifugation step. MNs containing 50% of the OVA and poly(I:C) dose encapsulated in NPs and 50% in free form (free-OVA-PIC/NP mixture) were prepared similarly to NP-loaded MNs but with some modifications. Free OVA (5 mg/ml) and poly(I:C) (5 mg/ml) were mixed to form the mixture for preparation of MN tips with HA (20 mg/ml) and subsequently NPs (2.5 mg/ml) were added to this mixture. The HA solution for backplate contained OVA (5 mg/ml) and poly(I:C) (5 mg/ml). Subsequently, the samples were dried overnight in a vacuum desiccator at room temperature. Finally, the vinylpolysiloxane backplate was prepared as described above.

2.5. Microscopic analysis of microneedles

The shape of MNs after the preparation and after the immunisation experiments were analysed by light microscopy (Zeiss, Sterni 2000 C, Carl Zeiss Microscopy GmbH, Göttingen, Germany). Scanning electron microscopy (SEM, NOVA nanoSEM, Eindhoven, the Netherlands) was used to examine additionally the shape, and external and internal surface morphology of the MNs. The arrays were coated with a platina/palladium layer to increase the surface conductivity. Images were taken at magnifications of 31–15,000× by using a voltage of 15 kV between the electron gun and the sample surface.

The distribution of the NPs containing OVA-AF647 in MNs with FAM-HA were analysed with fluorescence microscopy (Zeiss Imager D2, camera AxioCam MRm, light source HXP120V, Carl Zeiss Microscopy GmbH, Göttingen, Germany) before and after dissolution in the *ex vivo* human skin. ZEN Pro 2012 software (Carl Zeiss Microscopy GmbH) was used for imaging and image analysis in light and fluorescence microscopy.

2.6. Reconstitution of PLGA nanoparticles after microneedle dissolution

To examine whether the various steps of MN preparation influence the release of the NPs from the MNs upon the MN dissolution, asymmetrical flow field-flow fractionation (AF4) was utilized. The following samples were prepared: (1) NP suspension, (2) NP suspension with HA, (3) NP suspension with HA dried at +37 °C in ambient pressure, (4) NP suspension with HA dried at room temperature in vacuum and (5) NP-loaded MNs without silicone backplate. In all samples the NP:HA weight ratio was 1:4 and 10% of total HA was replaced with FAM-HA. After drying samples 3 and 4, and 5 on the flat PDMS surface or in PDMS mold, respectively, they were dispersed and dissolved in PBS (pH 7.4) overnight at +37 °C. Before the analysis, all samples were diluted to a concentration of 1 mg/ml NPs and 4 mg/ml HA in PBS.

The AF4 measurements were performed on an Agilent 1200 system (Agilent Technologies, Palo Alto, CA, USA) combined with Wyatt Eclipse detectors (Wyatt Technology Europe GmbH, Dernbach, German). For the separation of NPs and HA, a small channel equipped with a 350 μm spacer of medium width and a regenerated cellulose membrane with a cut-off of 5 kDa were used. Multiangle laser light scattering (MALLS) was used for the detection of the NPs and the fluorescence signal (λ_{ex} 496 nm, λ_{em} 520 nm) for the FAM-HA. The mobile phase was 200 mM $NaNO_3$ with 0.02% NaN_3, filtered through a 0.1 μm filter. The injection volume was 20 μl per sample and the detector flow was 1 ml/min. The cross-flow was initially set to 0.3 ml/min which was gradually decreased to 0.1 (from 9 to 12 min), and set at 0.1 ml/min until 32 min thereafter to 0 ml/min as indicated in Fig. 4A. The fractions were collected at 16–21 min and the particle size of the NPs of the fractions were measured with DLS as described above.

2.7. In vitro quantification of PLGA NPs and free OVA content of dissolving MNs

For this experiment, MNs were prepared as described above except that NP-loaded MNs contained NPs encapsulating OVA-IR800 and for OVA MNs 5% of the total OVA was replaced with OVA-AF647. Each array (n = 9 and n = 6 for NP and OVA-loaded MNs, respectively) was dispersed in 1 ml of PBS (pH 7.4) for 2 h and the NP and OVA content was determined with a Tecan plate reader based on the fluorescence of OVA-IR800 (λ_{ex} 779 nm, λ_{em} 794 nm) and OVA-AF647 (λ_{ex} 650 nm, λ_{em} 668 nm), respectively.

2.8. Dissolving MN penetration and dissolution in ex vivo human skin

Ex vivo human skin was used to analyse the penetration and dissolution of dissolving MN in the skin. Within 24 h after the skin was obtained from the hospital, excess fat was removed and the skin was

frozen and stored at −80 °C until use. Upon use, the skin was thawed and fixed on the Styrofoam. The MNs were applied onto the skin by using an in-house developed impact-insertion applicator [26] by attaching MN array to the applicator head with double-sided tape before application to the skin.

In the case of skin piercing studies, after inserting MNs into the skin for 15 s, 50 µl of 0.4% (w/v) trypan blue solution was applied onto the skin surface for 30 min [24]. After the removal of trypan blue solution, the skin was cleaned with MQ water to avoid visualization of trypan blue at the skin surface, and finally the stratum corneum was removed by tape stripping (~10 strips) by using normal office tape. The skin piercing indicated by blue spots was visualised with a light microscope (Zeiss, Sterni 2000 C) and the penetration efficiency was calculated diving the number of the successful piercings with the total number of tips (i.e. 16) in each MN array.

For dissolution studies, MNs were applied onto the skin for 20 min as described for penetration studies. After withdrawal, the MNs were analysed with a fluorescence microscope. To examine the deposition of NPs and HA into the skin, this was analysed after MN dissolution with confocal laser scanning microscopy as described previously [24]. Briefly, the experiment was carried out with a Nikon T-200-e inverted microscope supplied with a Nikon C1 confocal unit. For acquisition and analysis of scans, a Nikon Plan Apo 4 × (numerical aperture 4) objective and Nikon NIS Elements version 4.20.00 64-bit software were used. The *xy* resolution was 6.3 µm/pixel and *xy* scans were acquired every 10 µm, and rhodamine-labelled trimethyl chitosan (TMC) [27] was used to determine the skin surface during the analysis. NPs (i.e. AF647-OVA in NPs) and FAM-HA were visualised with a 637 nm (diode laser, intensity 75 and gain 100) and a 488 nm (Ar laser, intensity 75 and gain 100) laser, respectively.

2.9. Animals

Balb/c mice (haplotype $H2^d$, female, age 7–8 weeks) and C57BL/6 mice ($CD45.2^+$, $H2^b$, age 8 weeks) were purchased from Charles Rivers (Maastricht, The Netherlands). They were housed under standardised conditions in the animal facility of Leiden Academic Centre for Drug Research of Leiden University. Experiments were approved by the ethical committee on animal experiments of Leiden University (licence number 14241).

2.10. Quantification of the delivered dose by dissolving microneedles in vivo

Dissolving MNs containing NPs encapsulating IR800-OVA or free IR800-OVA were used to quantify amount of delivered OVA-NPs and OVA in the skin, respectively. First, balb/c mice were anaesthetised by intraperitoneal injection of ketamine (60 mg/kg) and xylanize (4 mg/kg) and the insertion site was shaved. Next, MNs were applied on by using an impact-insertion applicator for 20 min, as described above (Section 2.8). The calibration standards were injected with a hollow MN applicator as described below (Section 2.11) in shaved *ex vivo* mouse skin by using either free IR800-OVA (63–1000 ng protein/injection) or IR800-OVA-NPs (0.625–20 µg NPs/injection). The variation of injected amount of OVA or NPs was achieved by varying the injection volume (0.31–10 µl). Mice were sacrificed before measuring the fluorescence intensity by using a Perkin-Elmer IVIS Lumina Series III *in vivo* imaging system (Waltham, MA, USA) with an excitation wavelength of 745 nm and an emission filter set at ICG. Other parameters were set as follows: acquisition time 8 s, F-stop 2, binning 4 and field of view of 12.5 cm. Perkin-Elmer Living Image software version 4.3.1.0 was used for image acquisition and analysis. Untreated sites of the skin were used to determine the background signal.

2.11. Immunisation study for antibody responses

Study groups (n = 8/group) were immunised either by intradermal injection with hollow MNs or 20 min insertion of dissolving MNs on the flank of the mice. Hollow MNs were fabricated by hydrofluoric acid etching from fused silica capillaries and injections were performed with an in-house developed applicator as described earlier [20,28,29]. The bore diameter of the hollow MNs was 50 µm, the injection depth 200 µm, the injection rate 12 µl/min and the injection volume 12 µl. Before the immunisation, mice were anaesthetised by intraperitoneal injection of ketamine (60 mg/kg) and xylanize (4 mg/kg) that was followed by the shaving of the immunisation site. In all study groups, the total dose of both OVA and poly(I:C) doses were ~1 µg. Three different formulations were used and they were administered with both hollow and dissolving MNs: 1) free-OVA-PIC, 2) mixture of free-OVA-PIC (50% of dose) and OVA-PIC-NPs (50% of dose), and 3) OVA-PIC-NPs. The buffer with low ion concentration (10 mM phosphate buffer, pH 7.0) was used to dissolve OVA and poly(I:C), and to suspend NPs to prevent a premature release from NPs. Mice were immunised on the day 0 (prime), day 21 (1st boost) and day 42 (2nd boost), and before each immunisation venous blood sample was collected from the tail to measure the antibody responses. Mice were sacrificed on day 51 by first collecting a blood sample from abdominal/thoracic vein followed by cervical dislocation.

2.12. ELISA analysis of OVA-specific IgG antibodies

OVA-specific antibodies were analysed by a sandwich enzyme-linked immunosorbent assay (ELISA) as described earlier [20]. The plates (Nunc-Immuno MaxiSorp 96, ThermoScientific, Roskilde, Denmark) were coated with 500 ng of OVA for 1.5 h at 37 °C in 0.05 M carbonate/bicarbonate buffer (pH 9.6), followed by the blocking step with 1% (w/v) BSA in PBS (1 h at 37 °C). Next, diluted sera of each mouse was further serially diluted three-fold with dilution buffer (PBS with 0.5% BSA and 0.05% Tween 80) and incubated for 1.5 h at 37 °C. Subsequently, 1:5000 diluted horseradish peroxidase-conjugated goat antibodies against IgG, IgG1, IgG2a were added to the plates to be incubated for 1.5 h at 37 °C. Finally, antibodies were detected by adding TMB and after 15 min, the reaction was stopped with 2 M H_2SO_4. The absorbance was measured at 450 nm and the antibody titre was determined as a log10 value of the mid-point dilution of S-shaped dilution-absorbance curve of the diluted serum level.

2.13. Immunisation study for transgenic $CD4^+$ and $CD8^+$ T-cell responses

One day before the immunisation, $CD8^+$ T cells (OT-I, $CD45.1^+$) and $CD4^+$ T cells (OT-II, $CD45.1^+$) were obtained from transgenic mice as described recently [20]. An equivalent 20 000 OT-I and 200 000 OT-II cells were adoptively transferred in the C57BL/6 mice ($CD45.2^+$, $H2^b$) by i.v. injection in 200 µl PBS. On the following day, mice (n = 4/group) were immunised with OVA-PIC-NPs (OVA and poly(I:C) doses ~ 4 µg) either delivered by using four dissolving MN arrays per mouse or hollow MNs as described above. PBS was injected by hollow MNs for the negative control group (n = 3). At day 7, mice were sacrificed by cervical dislocation and spleens were collected to isolate splenocytes for flow cytometry analysis.

2.14. Flow cytometry analysis of $CD8^+$ and $CD4^+$ T-cells

Splenocytes were isolated from the collected spleens by using 70 µm Nylon cell strainers (Falcon, Corning, Corning, NY, USA) followed by 30 s lysis of erythrocytes by using Ammonium-Chloride-Potassium (ACK) lysis buffer. Thereafter, the splenocytes were washed with PBS and cell suspension (~500 000 cells per well) was added to the 96-well plate. After the washing of the cells, the cell surfaces were stained with fluorescently labelled antibodies against CD45.1 (efluor450, 1:800 dilution), CD4 (APC, 1:800), CD8α (PE, 1:800) and Thy1.2 (PE-Cy7, 1:400) in 100 µl of FACS buffer. After 30 min incubation at +4 °C, the excess antibodies were washed by FACS buffer before the incubation

with Cytofix solution (BD Bioscience) for 10 min at 4 °C. Before the flow cytometry analysis (FACS CantoII, BD Biosciences), the cells were washed once with FACS buffer. The data were analysed by using FlowJo software (version 10.0.7. TreeStar Inc).

2.15. Statistical methods

Statistical differences in immunisation studies were analysed by 1-way ANOVA with Bonferroni's multiple comparison post-test (GraphPad Prism version 5.02). The data of DLS analysis of AF4 fractions was analysed by Kruskall-Wallis test followed by Dunn's multiple comparison test. The level of the significance was set at 0.05 in both cases.

3. Results

3.1. Development and characterisation of PLGA NP-loaded dissolving MNs

PLGA NPs were loaded with OVA (OVA-NP) for MN development and characterisation studies, and with OVA and poly(I:C) (OVA-PIC-NP) for immunisation studies. The NPs had a size, determined by DLS and expressed as Z-average diameter, between 150 and 200 nm and their zeta potential was negative (Table 1). The co-encapsulation of poly(I:C) did not significantly affect these values. The OVA loading capacity in OVA-NPs was 7.7% w/w and the encapsulation efficiency was 67%. When OVA and poly(I:C) were co-encapsulated, their loading capacities were 3.2% and 3.0% (w/w), respectively, and thus the weight ratio of their encapsulated doses was approximately 1:1. The difference in OVA loading capacity between OVA-NPs and OVA-PIC-NPs was probably due to adjustment of initial amount of OVA in order to obtain equal loading capacity of OVA and poly(I:C). The encapsulation efficiencies of OVA and poly(I:C) in OVA-PIC-NPs were 53% and 10%, respectively.

HA-based dissolving MNs containing antigen and adjuvant loaded NPs were successfully developed. Preliminary studies indicated that sharp MNs with very high NP content could be produced without additional HA as matrix material in the MN tips (data not shown). However, these MNs did not have sufficient mechanical strength for reproducible skin penetrations. Consequently, it was decided to mix varying concentrations of HA solution with the NP suspension to study which compositions result in the formation of MNs with sufficient strength and sharpness for skin penetration. The examined weight ratios of NP:HA were 1:1, 1:4 and 1:10. During the preparation, the first four preparation steps was repeated once to increase the number of NPs deposited into the MN tips and consequently to increase the dose delivered into the skin (Fig. 1). All MNs (containing NPs, free-OVA-PIC/NP mixture, or free-OVA-PIC) had equal dimensions (length 300 μm) and sharpness (Fig. 2).

To minimize wastage of vaccine and increase the delivered dose, it is crucial that NPs are localized in the MN tips and minimally in the backplate. As can be inferred from SEM (Fig. 2) and fluorescence imaging (Fig. 3), the NPs were mainly concentrated in the tips of the MNs. SEM images showed that the upper parts of the MN tips had rough surfaces (Fig. 2A–C) in contrast to smooth surfaces of MNs with free-OVA-PIC (Fig. 2E), suggesting the localization of NPs into the MN tips. Additionally, fluorescence microscope images showed that low HA concentrations (10 or 20 mg/ml, with a NP:HA weight ratio of 1:1 and 1:4, respectively) allowed the efficient deposition of NPs into the MNs tips. This is indicated by the yellow colour of the MN tips, resulting from overlay of OVA-AF647 loaded NPs (red label) and FAM-HA (green label) (Fig. 3A and C). Furthermore, fluorescence microscope images suggested that the NP content of MN tips was relatively uniformly distributed between different MN tips with 1:4 and 1:1 NP:HA ratios (Fig. 3A and C). In contrast, a high HA concentration (50 mg/ml) with 1:10 NP:HA ratio seems to prevent the homogenous NP distribution in the MN tips or backplate (Figs. 2C and 3E) due to the high viscosity caused by the elevated HA concentration. Finally, SEM images of cross-sections cut at the approximate half-height of MN tips were analysed. The comparison of the cross-sections of OVA-loaded and NP-loaded MNs indicated the presence of NPs in the HA matrix of NP-loaded MNs (Fig. 2G–H). Spherical shapes of NPs could be detected in the cross-sections of NP-loaded MNs, while OVA-loaded MNs had smooth cross-section surface.

After NP-loaded MNs have been applied into the skin, they should be able to release the NPs in non-aggregated form. Since it would be very difficult to study the particle size of NPs released *in situ* in skin, we decided to dissolve the MNs in PBS instead and analysed the size of the released NPs by AF4 and DLS. As the NP:HA 1:4 ratio had the most optimal characteristics concerning NP distribution and dissolution in the skin (see next Section 3.2), we selected this ratio for the experiments. AF4 was used to separate FAM-labelled HA and (unlabelled) NPs and analyse the samples with online fluorescence and MALLS detection, respectively. Based on the MALLS signal, it was selected which fractions were collected from AF4 analysis to measure NP size offline with DLS. In addition, the MALLS signal was used to compare the relative amounts of particulate material in AF4 elugrams between different samples prepared with same NP batches [30]. However, there are limitations in the use of MALLS signal since it is affected not only by particle concentration but also by the particle size. Alternatively, refractive index signal could be used but in this study the signal was too weak for meaningful analysis.

First, the fluorescence signal of FAM-labelled HA was similar in all samples containing NPs, suggesting that different drying conditions did not affect HA dissolution (Fig. 4A). HA without NPs had the elution peak maximum at 9 min but in the presence of NPs the elution peak shifted to 12 min. However, the elution peaks of samples containing NPs had shoulder at 9 min. This indicates that in samples containing NPs, a part of HA is in original form while other part of HA was weakly interacting with NPs. As expected, the NP suspension showed a practically flat fluorescence baseline.

According to the MALLS signal, the NPs started eluting at 12 min. Thus, it was not overlapping with the elution of HA, and additionally HA did not show a measurable MALLS signal (cf. Fig. 4A and B). The MALLS signal was high for non-dried NP control samples, i.e., NP suspensions with and without HA, but the presence of HA slightly delayed the elution of NPs (Fig. 4B), confirming the presence of interaction between the NPs and HA. NP:HA samples dried in a vacuum desiccator at room temperature had a high and similar MALLS signal to that of

Table 1
Physicochemical properties and OVA and poly(I:C) loading characteristics of OVA-NPs (mean ± SD, n = 4) used for *in vitro* studies and OVA-PIC-NPs (n = 5) used in immunisation studies.

Formulation	Size (nm)[a]	PDI	Zeta potential (mV)	OVA LC[b] (% w/w)	Poly (I:C) LC[a] (% w/w)	OVA EE[c]%	Poly(I:C) EE[c] %
OVA-NP	187 ± 31	0.25 ± 0.05	−18.1 ± 4.4	7.7 ± 0.4	N/A	66.7 ± 3.5	N/A
OVA-PIC-NP	160 ± 12	0.16 ± 0.03	−12.0 ± 4.6	3.2 ± 0.9	3.0 ± 2.2	53.3 ± 10.7	10.5 ± 6.7

N/A = not applicable.
[a] Z-average.
[b] loading capacity.
[c] encapsulation efficiency.

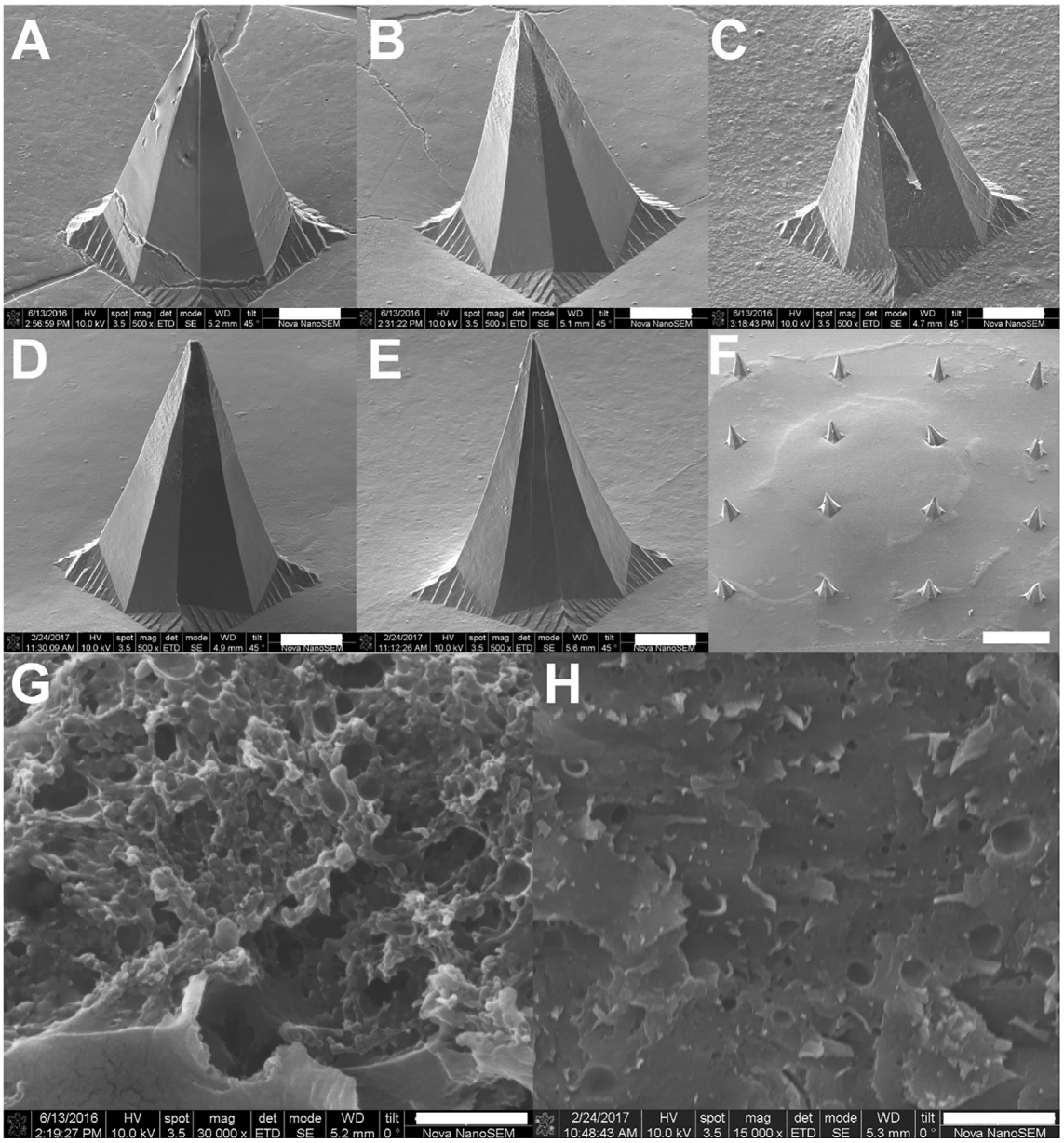

Fig. 2. SEM images of, single tips of MNs with 1:1 (A), 1:4 (B) and 1:10 (C) NP:HA ratios, and MN tips of free-OVA-PIC/NP mixture (D) and free-OVA-PIC (E), full array of NP-loaded MN 1:4 NP:HA ratio (F), and cross-sections of NP-loaded MNs (1:4 ratio) (G) and free-OVA-PIC (H) MNs. Scale bars are 50 μm (A-E), 1 mm (F), 1 μm (G) and 2 μm (H).

(freshly prepared) NP:HA suspension. In contrast, NP:HA mixtures dried at 37 °C in ambient pressure showed a low MALLS signal upon reconstitution in PBS. These findings suggest that vacuum drying leads to minimal NP aggregation, whereas drying at ambient pressure conditions leads to substantial NP aggregation. This aggregation was also visually observed by the presence of precipitated material at the bottom of the sample vial. Next, the MALLS signal of dispersed MN samples largely overlapped with that of vacuum dried samples, suggesting the presence of dispersed NPs. However, the elution of NPs was delayed compared to the vacuum dried sample. Furthermore, when the cross-flow was stopped at 32 min, a higher amount of NPs or alternatively some very large of non-eluted particles were flushed out of the channel in comparison to vacuum dried samples. These observations suggest that eluted NPs in MN samples had a larger hydrodynamic diameter than NPs in the vacuum dried samples, which can be considered as an indication of the formation of NP aggregates. However, as mentioned above, the results indicate transient HA-NP complexes dissociating during the analysis, and not strong interactions between HA and NP.

DLS analysis of collected NP fractions from AF4 corroborated the above-presented AF4-MALLS results (Table 2). Compared to AF4-MALLS, DLS allows a more accurate quantification of the particle size. Mixing of HA solution and NPs did not affect the particle size of the NPs. Vacuum drying increased the particle size and PDI of the NPs only slightly (201 nm, 0.27), but after drying at ambient conditions (at 37 °C), the light scattering signal was very low and no meaningful DLS results could be obtained. This latter observation indicates a low concentration of NPs in the samples. In dispersed NP-loaded MN samples, the NP size and PDI, and were higher (287 nm, 0.35) than that of vacuum dried samples (201 nm, 0.27), and additionally the variation between separate experiments was larger as indicated by larger SD. This suggests that NPs were more aggregated in MN samples than in vacuum dried samples. This could be due to the centrifugation step during the MN preparation. Centrifugation does force NPs into the microcavities of the PDMS mold and this may have caused the NP aggregation.

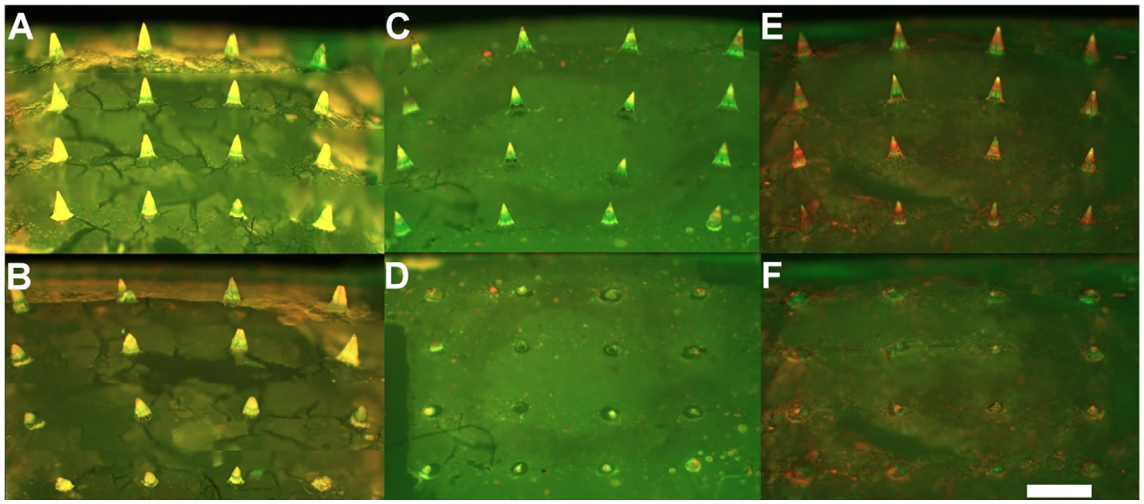

Fig. 3. NP-loaded MN arrays imaged with fluorescence microscopy before (A, C and E) and after 20 min (B, D and F) application into *ex vivo* human skin. Results for MN arrays prepared with NP:HA ratios of 1:1 (A-B), 1:4 (C-D) and 1:10 (E-F) are shown. Green, red and yellow colours indicate HA, OVA-AF647 loaded NPs and their co-location, respectively. The scale bar is 1 mm. (For interpretation of the references to colour in this figure legend, the reader is referred to the web version of this article.)

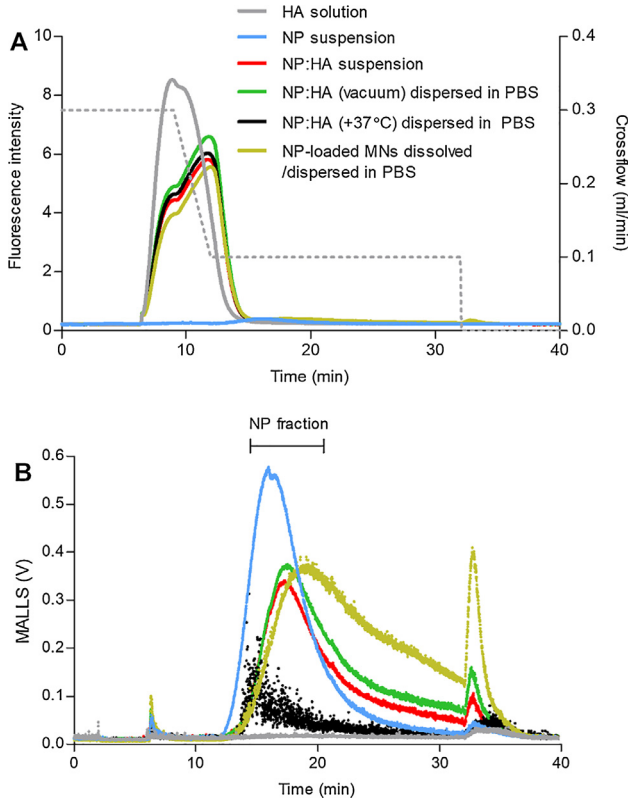

Fig. 4. AF4 elugrams of (A) FAM-labelled HA (measured by fluorescence) and (B) PLGA NPs (measured by MALLS) of dissolved MN sample and control samples. Both signals were recorded simultaneously but for sake of clarity the data is presented in two panels. In panel A, the crossflow profile is indicated by the dashed line (right y-axis) and in panel B, the period during which the NP fraction was collected for DLS analysis is indicated. All NP:HA samples had a weight ratio of 1:4 and samples are described in detail in Section 2.7. One representative set of elugrams from three independent experiments is presented. Legend in panel B as presented in panel A.

3.2. Dissolving MN piercing and dissolution in ex vivo human skin

Dissolving MNs need to have sufficient mechanical strength to penetrate into the skin and therefore their penetration into *ex vivo* human skin was examined by using a trypan blue assay. The skin penetration efficiency indicates the percentage of MN tips successfully penetrated into the skin and it was 91.9 ± 1.6% (n = 10), 100% (n = 6) and 85.4 ± 2.5% (n = 3) for MNs with NP:HA 1:1, 1:4 and 1:10 wt ratios, respectively (Fig. 5A). This experiment showed an excellent skin penetration efficiency for the different arrays, and especially for the MNs with a NP:HA weight ratio of 1:4.

Dissolution of the MNs with NP:HA ratios of 1:1, 1:4 and 1:10 was examined by assessing MN tips with microscope after the application into the *ex vivo* human skin. The NP:HA ratio remarkably influenced the dissolution of MN tips. For MNs with a NP:HA ratio of 1:1, the dissolution rate was slow and no significant dissolution occurred within 20 min (Fig. 3B). Importantly, the dissolution rate was clearly improved for MNs with 1:4 and 1:10 NP:HA ratios (Fig. 3D and F) and thus, an increase of HA content facilitated the MN dissolution. Finally, the skin was analysed with confocal microscopy immediately after the MNs were inserted and left for 20 min in the skin. The results showed that both the HA and the NPs were deposited into the *ex vivo* human skin until an approximate depth of 200–300 μm (Fig. 5B and C). Based on the results regarding the preparation of MNs and their dissolution, MNs with a NP:HA ratio of 1:4 were selected for *in vivo* studies.

Table 2
Z-average diameter and PDI (mean ± SD; n = 3–4) of fractions collected from AF4 analysis (16–21 min, see Fig. 4) and measured with DLS. All NP:HA samples had weight ratio of 1:4 and samples are described in detail in Section 2.7.

Sample	Z-average (nm)	PDI
NP suspension	174 ± 17	0.190 ± 0.077
NP:HA suspension	169 ± 12	0.228 ± 0.065
NP:HA (vacuum dried) dispersed in PBS	201 ± 34	0.272 ± 0.057
NP:HA (dried at 37 °C) dispersed in PBS	> 1000***	0.613 ± 0.292**
NP-loaded MNs dissolved/dispersed in PBS	287 ± 130*	0.350 ± 0.148

* $p < 0.05$ difference to NP:HA suspension.
** $p < 0.01$.
*** $p < 0.001$.

3.3. Dissolution rate and delivered antigen dose of dissolving MNs in mice

The MN dissolution rate and antigen dose delivered into the skin were characterised *in vivo* in mice after administering dissolving MNs containing NPs (NP:HA ratio 1:4) loaded with OVA-IR800. The MNs were applied into the skin of mice (n = 4) and left in the skin for 20 min

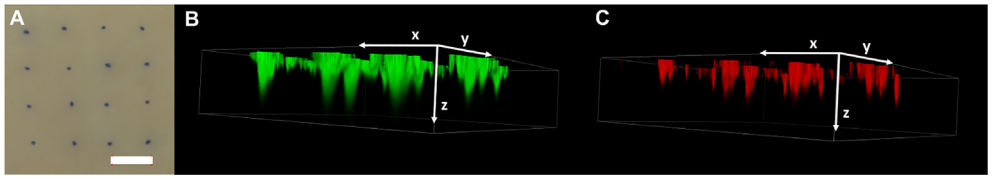

Fig. 5. A representative top view of *ex vivo* human skin indicating the penetration of dissolving MNs (NP:HA ratio 1:4) into the skin, the scale bar is 1000 μm (A); confocal microscopy images showing the deposition of HA in green (B) and NPs in red (C) into *ex vivo* human skin after 20 min application of MNs (NP:HA ratio 1:4), with the x- and y-axis indicating the skin surface, and the z-axis (length 700 μm) the depth of the skin. (For interpretation of the references to colour in this figure legend, the reader is referred to the web version of this article.)

by using an impact-insertion applicator, similarly to the experiments with *ex vivo* human skin. The delivered dose of antigen was quantified by near-IR imaging [23]. Hollow MN injections of OVA-IR800 loaded NPs were used for calibration, since the encapsulated OVA-IR800 had a significantly lower fluorescence signal than OVA-IR800 solution. NP-loaded MNs delivered 31.0 ± 14.3 μg (n = 7, mean ± SD) NPs into the mice, which corresponds to 0.99 ± 0.46 μg OVA and 0.93 ± 0.43 μg poly(I:C) based on loading capacities of OVA-PIC-NPs used for immunisation studies (Table 1). When the delivered dose of NPs was compared to NP content of total MN array (130 ± 25 μg, n = 9, mean ± SD) measured *in vitro*, it was found that 24% of the dose contained in NP-loaded MN arrays was actually delivered into the skin.

In the case of MNs containing free-OVA, injections of free OVA-IR800 were used for calibration. These MNs delivered 1.02 ± 0.52 μg (n = 5, mean ± SD) OVA into the mice. The delivered poly(I:C) dose was not measured, but is expected to be approximately 1 μg based on the OVA:poly(I:C) ratio of 1:1 in the MNs. OVA-loaded MN arrays contained totally 652 ± 57 μg (n = 6, mean ± SD) OVA based on *in vitro* dissolution experiment. Consequently, only 0.16% of the total OVA in a MN array was delivered into the skin. Therefore, it can be concluded that NP-loaded MNs had much higher delivery efficiency into the skin than free-OVA loaded MN arrays, and that the wastage of the payload was moderate in NP-loaded MNs. Nevertheless, it must be noted that a part of the antigen is lost during the NP fabrication since the encapsulation efficiency is not 100%. For MNs containing a mixture of free OVA and NPs, it was assumed that MNs would have a similar delivery efficiency of NPs and free-OVA as MNs containing solely NPs or free-OVA.

3.4. Immunisation studies

Mice were immunised with OVA-PIC-NPs, a solution of OVA and poly(I:C) (free-OVA-PIC), or a 1:1 mixture of OVA-PIC-NPs and free-OVA-PIC administered either by dissolving MNs or a hollow MN. The major difference between these two immunisation methods is that a hollow MN delivers a known volume of either vaccine solution or suspension [20], whereas dissolving MNs are solid formulations requiring dissolution and release of vaccine.

All dissolving MN arrays were characterised by light microscopy after the immunisations studies (Fig. 6). These analyses confirmed that > 95% of applied arrays could dissolve sufficiently to deposit the MN tip containing NPs or free-OVA-PIC into the mice. Furthermore, the visual analysis of MNs after the immunization did not reveal any substantial differences between the dissolution of MNs containing (1) OVA-PIC-NPs, (2) free-OVA-PIC or (3) a mixture of these two.

In the case of immunization with soluble free-OVA-PIC, delivery with dissolving and hollow MNs resulted in comparable IgG1 and IgG2 responses (Fig. 7). When 50% of the OVA dose was in soluble form and the other 50% of the OVA loaded in NPs, hollow MN mediated delivery tended to evoke higher OVA specific IgG1 and IgG2a responses than dissolving MN mediated delivery, although no statistical differences were found. When the whole OVA dose was encapsulated in NPs, hollow MN mediated delivery resulted in statistically stronger IgG1 responses than NP-loaded dissolving MNs at all time points (Fig. 7). In addition, strong IgG2a response was detected after hollow MN-mediated delivery of NPs but not after the dissolving MN-mediated delivery. Moreover, in line with our previous results [20], encapsulation of OVA and poly(I:C) in NPs did not improve the IgG1 response, but was required for eliciting a robust IgG2a response after hollow MN mediated immunisation (Fig. 7D–F). An increased IgG2a response after NP vaccination suggests triggering of cellular immune responses. Therefore, $CD8^+$ and $CD4^+$ T-cell responses were analysed by using adoptive transfer of transgenic OT-I and OT-II cells before the delivery of the OVA-PIC-NPs by dissolving and hollow MNs. Hollow MN mediated delivery of NPs resulted in robust $CD8^+$ and $CD4^+$ T-cell responses (Fig. 8). In contrast, dissolving MN mediated delivery resulted in absence of a $CD8^+$ response and only a minimal $CD4^+$ response.

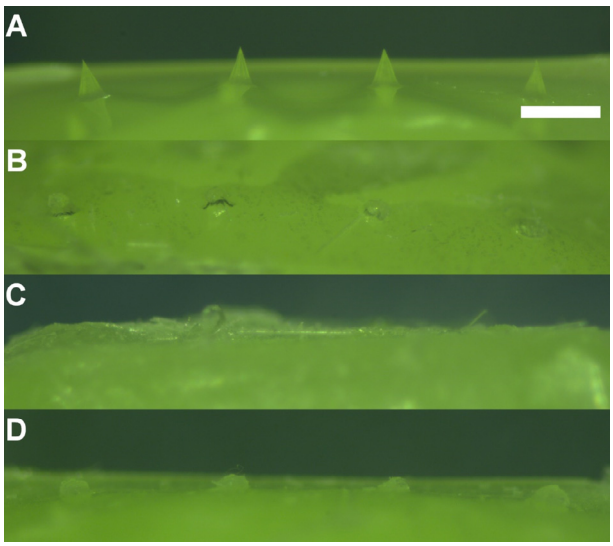

Fig. 6. Light microscopy images of dissolving MN arrays before (A) and after 20 min application to mice in immunisation studies: NP- (B), free-OVA-PIC/NP mixture- (C) and free OVA-PIC- (D) loaded MNs. All formulations dissolved *in vivo* in a comparable manner since no MN tips can be detected in panels B-D. The scale bar is 500 μm.

4. Discussion

The aim of the study was to develop a dry-state nanoparticulate vaccine formulation for minimally invasive intradermal immunisation by using HA-based MNs. The developed MNs should be able to penetrate into the skin followed by fast dissolution, and subsequently deliver a sufficient antigen dose in a reproducible manner. Until now, only a small number of studies have described the use of nano- [17,18,31] or microparticle [32] -loaded dissolving MNs for intradermal vaccine delivery. However, these studies were mainly focused on the analysis of immunological effects, whereas the understanding of optimal MN formulation parameters is still limited. Therefore, in this study, important technical aspects of the pharmaceutical development of such a complex formulation combining NPs and dissolving MNs were explored. The clinical translation of dissolving MNs for vaccination has been recently reviewed [4] and it is not further discussed here.

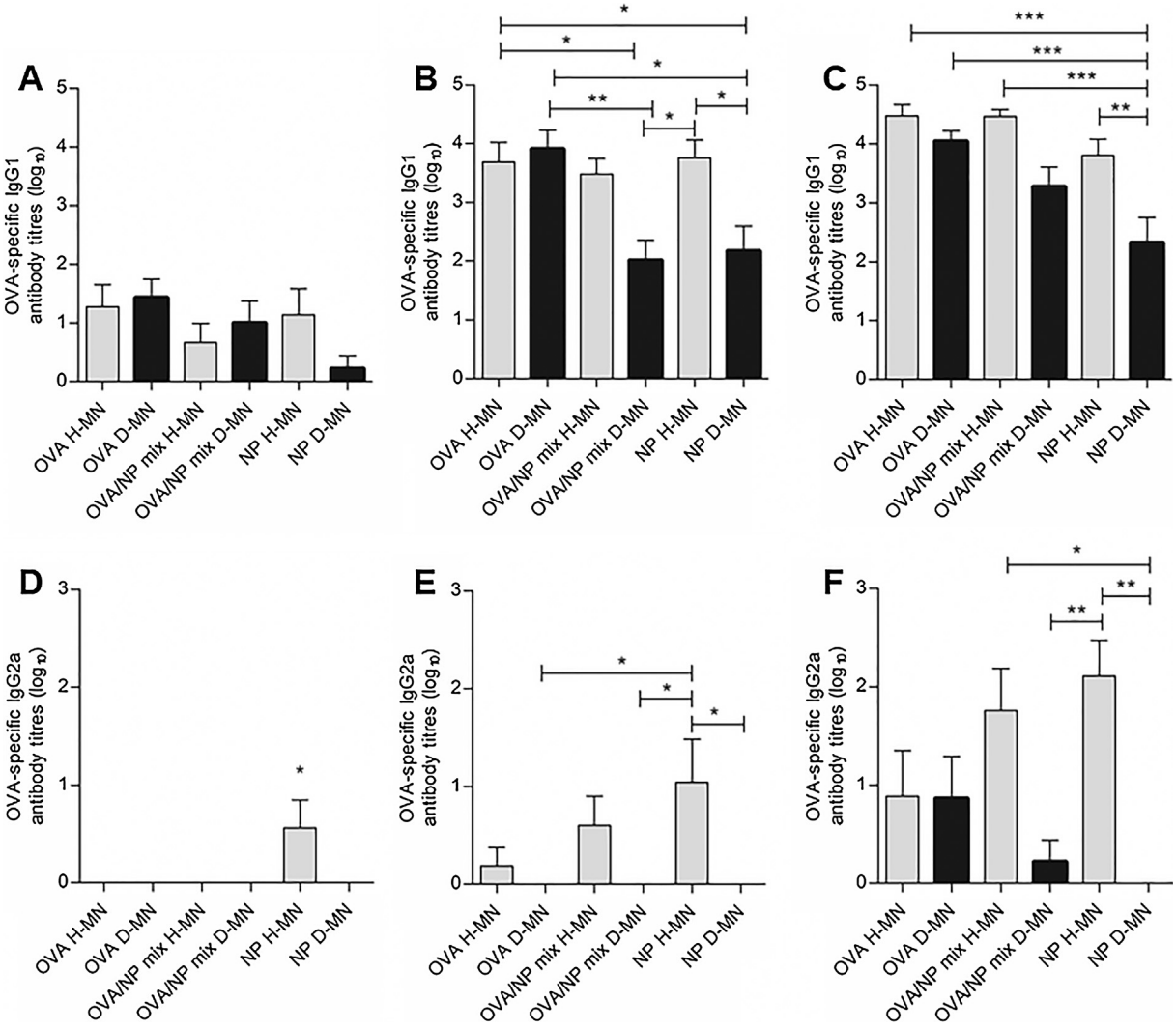

Fig. 7. IgG1 (A-C) and IgG2a (D-F) responses 21 days after the prime immunisation (A and D), 21 days after the boost (B and E) and 9 days after the second boost (C and F) administered with hollow MNs (H-MN, grey bars) or dissolving MNs (D-MNs, black bars). Mid-point titres $\log_{10}$ dilutions shown (mean ± SEM, n = 8). $^{*}p < 0.05$, $^{**}p < 0.01$, $^{***}p < 0.001$.

The ratio of HA as matrix material and NPs was found to be important for successful skin penetration and dissolution of MNs. The optimal NP:HA ratio obtained in this study was 1:4 and this was based on two observations. First, with a NP:HA weight ratio of 1:1 or 1:4, the viscosity of HA did not negatively affect MN preparation. In contrast, a high HA content of the MNs with NP:HA weight ratio 1:10 increased the viscosity of NP/HA suspension such that the suspension became difficult to handle in the preparation phase. In addition, the higher viscosity limited the deposition of NPs into the MN tips, as was reported also recently for PVP/PVA-based MNs [18]. Importantly, this can decrease the delivered vaccine dose. Secondly, MN dissolution in *ex vivo* human skin was strongly influenced by the NP:HA ratio. Whereas MNs with a NP:HA weight ratio of 1:4 or 1:10 dissolved within 20 min in the skin, those with a NP:HA ratio of 1:1 hardly dissolved and were therefore considered unsuitable for effective immunisation. Interestingly, MN dissolution in mouse skin was more complete than in *ex vivo* human skin, probably due to the higher humidity and temperature of the tissue of the mice. Based on the results of these studies, the dissolving MNs with a NP:HA weight ratio of 1:4 were selected for *in vivo* studies.

The centrifugation and drying conditions were found to be critical for successful MN preparation. Without the optimization of these conditions, it would not be possible to deliver sufficient vaccine into the skin and to ensure the ideal re-dispersion of NPs from dry-state to a single particle suspension in the skin, both of which are required for an effective immunisation. First, the centrifugation step was crucial to increase the delivered antigen dose by at least 100-fold, by depositing the NPs into the MN tips. This was estimated by comparing the percentages of the delivered dose of the total vaccine content of a MN arrays between free OVA and NP-loaded MNs (0.16% vs. 24%) since free OVA as solute is not deposited into MN tips by the centrifugation as occurs for NPs. However, centrifugation bears the risk of potential aggregation of NPs, as indicated in this study by a slight increase of the particle size and the PDI of the NPs after *in vitro* dispersion of MN arrays. To study this, it was necessary to develop a novel analysis method of NP-loaded MNs combining AF4 and DLS, since the analysis with more straightforward methods (e.g., nanoparticle tracking analysis or DLS only) were confounded by the presence of HA in the dispersion medium (data not shown). The application of this developed method is not limited only for NP-loaded MNs but it is suitable also for other formulations embedding NPs in matrices. Secondly, besides the centrifugation, the importance of optimal drying conditions for good NP dispersion after MN dissolution was highlighted in this study. Vacuum-drying of the MNs during the preparation prevented practically completely NP aggregation, while drying of the MN arrays at ambient conditions, that were found to suitable for HA-based protein-loaded dissolving MNs in our previous study [24], led to severe NP

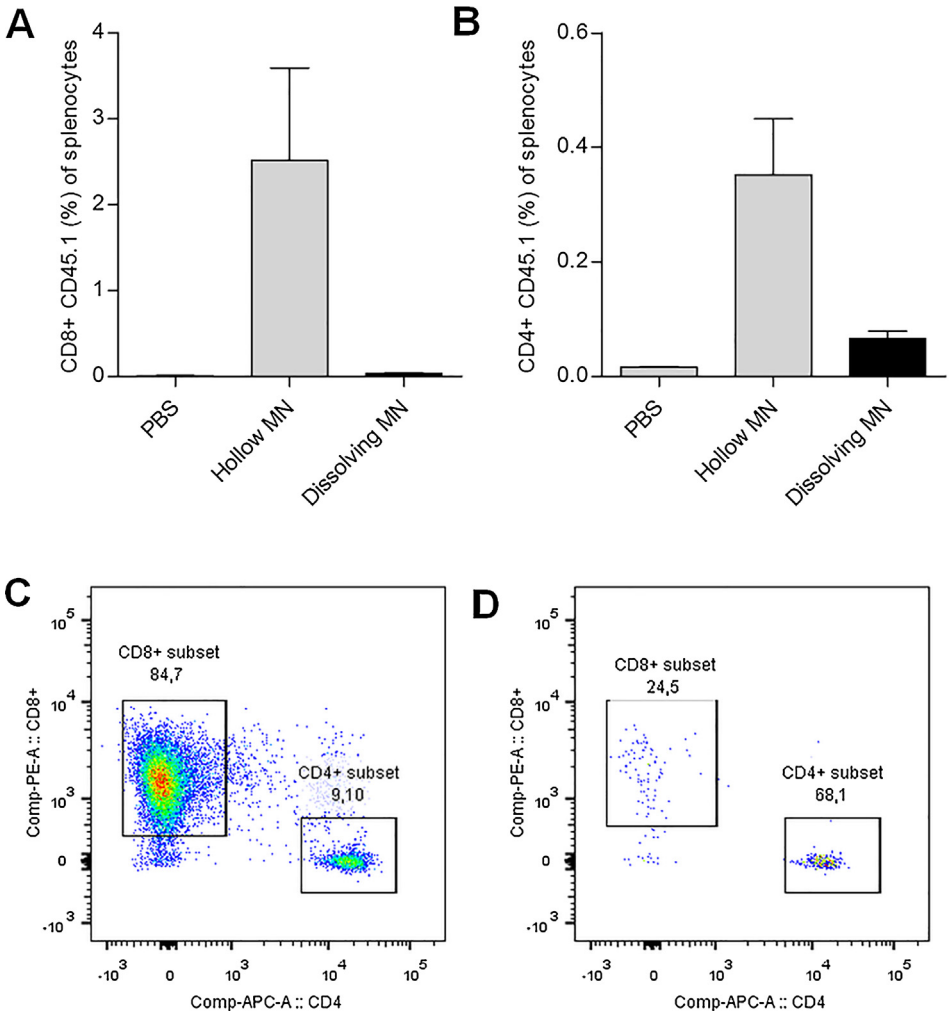

Fig. 8. Percentage of OVA specific $CD8^+$(A) and $CD4^+$T-cells (B) in splenocytes 7 days after immunisations with OVA-PIC-NPs shown (mean ± SEM, n = 4). Examples of CD45.1 pre-gated flow cytometry plots after hollow (C) and dissolving MN (D) immunisations are shown.

aggregation. The superiority of vacuum drying can be attributed a lower temperature and vacuum at low relatively humidity, which can decrease interactions between PLGA NPs and consequently susceptibility to the aggregation. However, as some NP aggregation was still detected after the *in vitro* dispersion of NP-loaded MNs, there is still room for further optimization such as by screening excipients or alternative drying methods. For example, freeze drying is generally used for drying of nanoparticles as dry powder [33] or when embedded in matrices [34]. Although, in the case of HA, freeze drying produces sponge-like cakes without sufficient mechanical strength for the penetration into the skin, it could be potentially suitable method for other matrix materials. Finally, it is highlighted that the optimization of preparation conditions should be performed for each NP and matrix combination.

Finally, the immunogenicity of dissolving MNs (dry state NPs) was compared to that of hollow MNs (NP suspension) using identical doses. The intradermal injection of OVA-PIC-NP suspension elicited strong cellular and humoral responses, which confirms our recent results showing the potency of this vaccine formulation [35]. Unfortunately, the NP-loaded dissolving MNs elicited inferior humoral responses and lacked cellular responses in comparison to hollow MN mediated immunization. However, immunisation with free-OVA-PIC by dissolving or hollow MN resulted in comparable immune responses, which suggests that the HA-based MNs are able to successfully deliver soluble antigens and adjuvants intradermally. Administration of a mixture of free and encapsulated OVA and poly(I:C) in dissolving MNs resulted in IgG1 responses between those of dissolving MNs containing either free antigen and adjuvant or antigen and adjuvant encapsulated in NPs. This supports the finding that OVA-PIC-NPs in dissolving MNs evoked inferior humoral responses compared to free-OVA-PIC. It is generally accepted that the nanoparticulate nature of the vaccine is required for strong T-cell and Th1-type responses since the NP uptake by dendritic cells is enhanced by small size (< 200 nm) [8,36] leading to co-delivery of antigen and adjuvant. Therefore, the absence of cellular or IgG2a immune responses in dissolving MN-mediated immunisation may be due to the absence or a low number of single NPs in the skin. As the MNs almost completely dissolved in the skin, our results suggest that NP-loaded dissolving MNs were unable to release NPs in non-aggregated form in the skin. This is different from the *in vitro* release analysed with AF4 and DLS. The discrepancy can be related to the differences between conditions *in vitro* and *in vivo* such as the limited amount of tissue fluid and low diffusivity in the skin as compared to PBS. Therefore, NP dispersion and distribution in the skin after the immunisation may be potentially hindered with dry vaccine formulation, such as dissolving MNs, leading to poor vaccine uptake by antigen presenting cells in comparison to administration of NP suspension.

For future studies, the formulation of dissolving MNs should be improved to maintain NP integrity upon release into the skin and to obtain T-cell responses, for instance, by examining suitable excipients and further optimizing the preparation conditions to enhance NP dispersion and distribution in the skin. Alternatively to PLGA NPs and HA, other MN matrix materials or nanoparticles, such as liposomes [15] and

nanogels [37,38], or use of antigen-adjuvant conjugates [39,40] could be examined, and thus more suitable formulations could be discovered.

5. Conclusions

HA-based dissolving MNs loaded with PLGA NP were developed for minimally invasive intradermal vaccination. The optimal ratio of NPs and HA in MNs was a critical parameter for MN preparation and dissolution in the *ex vivo* human skin. The importance of the drying conditions in the preparation of dissolving MNs was shown by AF4/DLS analysis of the NP size after *in vitro* dispersion of MNs. Intradermal immunisation with PLGA NP-loaded dissolving MNs was able to evoke humoral but practically no detectable cellular immune responses, whereas hollow MN mediated delivery of identical PLGA NPs resulted in robust humoral and cellular immune response. Finally, these results are a valuable foundation for the future development of MN-based delivery of particulate vaccines.

Acknowledgements

The research leading to these results has received support from the Innovative Medicines Initiative Joint Undertaking under grant agreement n° [115363], resources of which are composed of financial contribution from the European Union's Seventh Framework Programme (FP7/2007-2013) and EFPIA companies' in kind contribution.

References

[1] C. Levin, H. Perrin, B. Combadiere, Tailored immunity by skin antigen-presenting cells, Hum. Vaccines Immunother. 11 (2015) 27–36.
[2] K. Matsuo, S. Hirobe, N. Okada, S. Nakagawa, Frontiers of transcutaneous vaccination systems: novel technologies and devices for vaccine delivery, Vaccine 31 (2013) 2403–2415.
[3] K. van der Maaden, W. Jiskoot, J. Bouwstra, Microneedle technologies for (trans) dermal drug and vaccine delivery, J. Controlled Release. 161 (2012) 645–655.
[4] M. Leone, J. Mönkäre, J.A. Bouwstra, G. Kersten, Dissolving microneedle patches for dermal vaccination, Pharm. Res. 34 (2017) 2223–2240.
[5] S. Bobbala, S. Hook, Is there an optimal formulation and delivery strategy for subunit vaccines? Pharm. Res. 33 (2016) 2078–2097.
[6] G.J. Nabel, Designing tomorrow's vaccines, N. Engl. J. Med. 368 (2013) 551–560.
[7] C. Foged, J. Hansen, E.M. Agger, License to kill: formulation requirements for optimal priming of CD8+ CTL responses with particulate vaccine delivery systems, Eur. J. Pharm. Sci. 45 (2012) 482–491.
[8] M. Luo, L.Z. Samandi, Z. Wang, Z.J. Chen, J. Gao, Synthetic nanovaccines for immunotherapy, J. Controlled Release. 263 (2017) 200–210.
[9] L. Zhao, A. Seth, N. Wibowo, C.-X. Zhao, N. Mitter, C. Yu, A.P.J. Middelberg, Nanoparticle vaccines, Vaccine 32 (2014) 327–337.
[10] M.-L. De Temmerman, J. Rejman, J. Demeester, D.J. Irvine, B. Gander, S.C. De Smedt, Particulate vaccines: on the quest for optimal delivery and immune response, Drug Discov. Today 16 (2011) 569–582.
[11] S.P. Kasturi, I. Skountzou, R.A. Albrecht, D. Koutsonanos, T. Hua, H. Nakaya, R. Ravindran, S. Stewart, M. Alam, M. Kwissa, F. Villinger, N. Murthy, J. Steel, J. Jacob, R.J. Hogan, A. García-Sastre, R. Compans, B. Pulendran, Programming the magnitude and persistence of antibody responses with innate immunity, Nature 470 (2011) 543–547.
[12] M.T. Orr, E.A. Beebe, T.E. Hudson, J.J. Moon, C.B. Fox, S.G. Reed, R.N. Coler, A dual TLR agonist adjuvant enhances the immunogenicity and protective efficacy of the tuberculosis vaccine antigen ID93, PLOS One 9 (2014) e83884.
[13] S.L. Demento, N. Bonafé, W. Cui, S.M. Kaech, M.J. Caplan, E. Fikrig, M. Ledizet, T.M. Fahmy, TLR9-Targeted biodegradable nanoparticles as immunization vectors protect against west Nile encephalitis, J. Immunol. 185 (2010) 2989–2997.
[14] A. de Titta, M. Ballester, Z. Julier, C. Nembrini, L. Jeanbart, A.J. van der Vlies, M.A. Swartz, J.A. Hubbell, Nanoparticle conjugation of CpG enhances adjuvancy for cellular immunity and memory recall at low dose, Proc. Natl. Acad. Sci. 110 (2013) 19902–19907.
[15] E.M. Varypataki, N. Benne, J. Bouwstra, W. Jiskoot, F. Ossendorp, Efficient eradication of established tumors in mice with cationic liposome-based synthetic long-peptide vaccines, Cancer Immunol. Res. 5 (2017) 222–233.
[16] S. Hamdy, O. Molavi, Z. Ma, A. Haddadi, A. Alshamsan, Z. Gobti, S. Elhasi, J. Samuel, A. Lavasanifar, Co-delivery of cancer-associated antigen and Toll-like receptor 4 ligand in PLGA nanoparticles induces potent CD8+ T cell-mediated anti-tumor immunity, Vaccine 26 (2008) 5046–5057.
[17] M. Zaric, O. Lyubomska, O. Touzelet, C. Poux, S. Al-Zahrani, F. Fay, L. Wallace, D. Terhorst, B. Malissen, S. Henri, U.F. Power, C.J. Scott, R.F. Donnelly, A. Kissenpfennig, Skin dendritic cell targeting via microneedle arrays laden with antigen-encapsulated Poly-d, l-lactide-co-Glycolide nanoparticles induces efficient antitumor and antiviral immune responses, ACS Nano. 7 (2013) 2042–2055.
[18] H.-W. Yang, L. Ye, X.D. Guo, C. Yang, R.W. Compans, M.R. Prausnitz, Ebola vaccination using a DNA vaccine coated on PLGA-PLL/γPGA nanoparticles administered using a microneedle patch, Adv. Healthc. Mater. 6 (2017) 1600750.
[19] S.M. Caucheteux, J.P. Mitchell, M.O. Ivory, S. Hirosue, S. Hakobyan, G. Dolton, K. Ladell, K. Miners, D.A. Price, J. Kan-Mitchell, A.K. Sewell, F. Nestle, A. Moris, R.O. Karoo, J.C. Birchall, M.A. Swartz, J.A. Hubbel, F.P. Blanchet, V. Piguet, Polypropylene sulfide nanoparticle p24 vaccine promotes dendritic cell-mediated specific immune responses against HIV-1, J. Invest. Dermatol. 136 (2016) 1172–1181.
[20] G. Du, R.M. Hathout, M. Nasr, M.R. Nejadnik, J. Tu, R.I. Koning, A.J. Koster, B. Slütter, A. Kros, W. Jiskoot, J.A. Bouwstra, J. Mönkäre, Intradermal vaccination with hollow microneedles: a comparative study of various protein antigen and adjuvant encapsulated nanoparticles, J. Controlled Release. 266 (2017) 109–118.
[21] O.S. Kumru, S.B. Joshi, D.E. Smith, C.R. Middaugh, T. Prusik, D.B. Volkin, Vaccine instability in the cold chain: mechanisms, analysis and formulation strategies, Biologicals 42 (2014) 237–259.
[22] M.J. Mistilis, J.C. Joyce, E.S. Esser, I. Skountzou, R.W. Compans, A.S. Bommarius, M.R. Prausnitz, Long-term stability of influenza vaccine in a dissolving microneedle patch, Drug Deliv. Transl. Res. 7 (2017) 195–205.
[23] P. Schipper, K. van der Maaden, V. Groeneveld, M. Ruigrok, S. Romeijn, S. Uleman, C. Oomens, G. Kersten, W. Jiskoot, J. Bouwstra, Diphtheria toxoid and N-trimethyl chitosan layer-by-layer coated pH-sensitive microneedles induce potent immune responses upon dermal vaccination in mice, J. Controlled Release. 262 (2017) 28–36.
[24] J. Mönkäre, M. Reza Nejadnik, K. Baccouche, S. Romeijn, W. Jiskoot, J.A. Bouwstra, IgG-loaded hyaluronan-based dissolving microneedles for intradermal protein delivery, J. Controlled Release. 218 (2015) 53–62.
[25] M. Leone, M. Priester, J. Mönkäre, M.R. Nejadnik, C. O'Mahony, G. Kersten, J.A. Bouwstra, Unpublished results.
[26] K. van der Maaden, E. Sekerdag, W. Jiskoot, J. Bouwstra, Impact-insertion applicator improves reliability of skin penetration by solid microneedle arrays, AAPS J. 16 (2014) 681–684.
[27] S.M. Bal, Z. Ding, G.F.A. Kersten, W. Jiskoot, J.A. Bouwstra, Microneedle-based transcutaneous immunisation in mice with N-Trimethyl chitosan adjuvanted diphtheria toxoid formulations, Pharm. Res. 27 (2010) 1837–1847.
[28] K. van der Maaden, S.J. Trietsch, H. Kraan, E.M. Varypataki, S. Romeijn, R. Zwier, H.J. van der Linden, G. Kersten, T. Hankemeier, W. Jiskoot, J. Bouwstra, Novel hollow microneedle technology for depth-controlled microinjection-mediated dermal vaccination: a study with polio vaccine in rats, Pharm. Res. 31 (2014) 1846–1854.
[29] K. van der Maaden, J. Heuts, M. Camps, M. Pontier, A. Terwisscha van Scheltinga, W. Jiskoot, F. Ossendorp, J. Bouwstra, Hollow microneedle-mediated micro-injections of a liposomal HPV E743–63 synthetic long peptide vaccine for efficient induction of cytotoxic and T-helper responses, J. Controlled Release. 269 (2018) 347–354.
[30] A. Engel, M. Plöger, D. Mulac, K. Langer, Asymmetric flow field-flow fractionation (AF4) for the quantification of nanoparticle release from tablets during dissolution testing, Int. J. Pharm. 461 (2014) 137–144.
[31] M. Zaric, O. Lyubomska, C. Poux, M.L. Hanna, M.T. McCrudden, B. Malissen, R.J. Ingram, U.F. Power, C.J. Scott, R.F. Donnelly, A. Kissenpfennig, Dissolving microneedle delivery of nanoparticle-encapsulated antigen elicits efficient cross-priming and Th1 immune responses by murine langerhans cells, J. Invest. Dermatol. 135 (2015) 425–434.
[32] P.C. DeMuth, Y. Min, D.J. Irvine, P.T. Hammond, Implantable silk composite microneedles for programmable vaccine release kinetics and enhanced immunogenicity in transcutaneous immunization, Adv. Healthc. Mater. 3 (2014) 47–58.
[33] P. Fonte, S. Reis, B. Sarmento, Facts and evidences on the lyophilization of polymeric nanoparticles for drug delivery, J. Controlled Release. 225 (2016) 75–86.
[34] H. Valo, S. Arola, P. Laaksonen, M. Torkkeli, L. Peltonen, M.B. Linder, R. Serimaa, S. Kuga, J. Hirvonen, T. Laaksonen, Drug release from nanoparticles embedded in four different nanofibrillar cellulose aerogels, Eur. J. Pharm. Sci. 50 (2013) 69–77.
[35] A.M. de Groot, G. Du, J. Mönkäre, A.C.M. Platteel, F. Broere, J.A. Bouwstra, A.J.A.M. Sijts, Hollow microneedle-mediated intradermal delivery of model vaccine antigen-loaded PLGA nanoparticles elicits protective T cell-mediated immunity to an intracellular bacterium, J. Controlled Release. 266 (2017) 27–35.
[36] N. Benne, J. van Duijn, J. Kuiper, W. Jiskoot, B. Slütter, Orchestrating immune responses: How size, shape and rigidity affect the immunogenicity of particulate vaccines, J. Controlled Release. 234 (2016) 124–134.
[37] M. Toyoda, S. Hama, Y. Ikeda, Y. Nagasaki, K. Kogure, Anti-cancer vaccination by transdermal delivery of antigen peptide-loaded nanogels via iontophoresis, Int. J. Pharm. 483 (2015) 110–114.
[38] D. Li, F. Sun, M. Bourajjaj, Y. Chen, E.H. Pieters, J. Chen, J.B. van den Dikkenberg, B. Lou, M.G.M. Camps, F. Ossendorp, W.E. Hennink, T. Vermonden, C.F. van Nostrum, Strong in vivo antitumor responses induced by an antigen immobilized in nanogels via reducible bonds, Nanoscale 8 (2016) 19592–19604.
[39] Q. Huang, W. Yu, T. Hu, Potent antigen-adjuvant delivery system by conjugation of mycobacterium tuberculosis Ag85B-HspX fusion protein with arabinogalactan-poly (I:C) conjugate, Bioconjug. Chem. 27 (2016) 1165–1174.
[40] S.M. Bal, B. Slütter, W. Jiskoot, J.A. Bouwstra, Small is beautiful: N-trimethyl chitosan–ovalbumin conjugates for microneedle-based transcutaneous immunisation, Vaccine 29 (2011) 4025–4032.